

Influence of Metal Cations on the Viscoelastic Properties of *Escherichia coli* Biofilms

Adrien Sarlet, Valentin Ruffine, Kerstin G. Blank,* and Cécile M. Bidan*

Cite This: *ACS Omega* 2023, 8, 4667–4676

Read Online

ACCESS |



Metrics & More

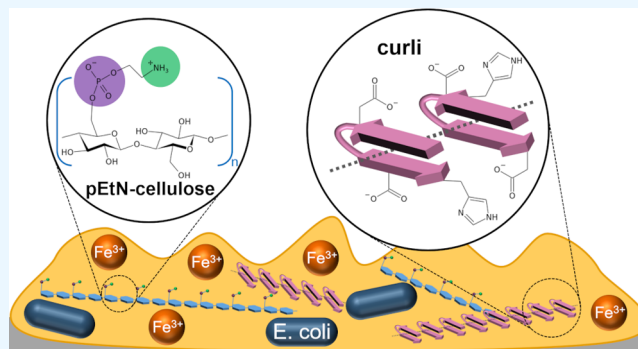


Article Recommendations



Supporting Information

ABSTRACT: Biofilms frequently cause complications in various areas of human life, e.g., in medicine and in the food industry. More recently, biofilms are discussed as new types of living materials with tunable mechanical properties. In particular, *Escherichia coli* produces a matrix composed of amyloid-forming curli and phosphoethanolamine-modified cellulose fibers in response to suboptimal environmental conditions. It is currently unknown how the interaction between these fibers contributes to the overall mechanical properties of the formed biofilms and if extrinsic control parameters can be utilized to manipulate these properties. Using shear rheology, we show that biofilms formed by the *E. coli* K-12 strain AR3110 stiffen by a factor of 2 when exposed to the trivalent metal cations Al(III) and Fe(III), while no such response is observed for the bivalent cations Zn(II) and Ca(II). Strains producing only one matrix component did not show any stiffening response to either cation or even a small softening. No stiffening response was further observed when strains producing only one type of fiber were co-cultured or simply mixed after biofilm growth. These results suggest that the *E. coli* biofilm matrix is a uniquely structured composite material when both matrix fibers are produced from the same bacterium. While the exact interaction mechanism between curli, phosphoethanolamine-modified cellulose, and trivalent metal cations is currently not known, our results highlight the potential of using extrinsic parameters to understand and control the interplay between biofilm structure and mechanical properties. This will ultimately aid in the development of better strategies for controlling biofilm growth.



INTRODUCTION

Biofilms are heterogeneous structures made of bacteria embedded in a self-secreted extracellular matrix. They cause complications in various fields of human life, e.g., in the medical sector,¹ the food industry,² and during wastewater treatment.³ To date, most biofilm research has focused on the development of preventive anti-biofilm strategies. More recently, biofilms have emerged as a potential source of sustainable materials. For example, biofilms were utilized for the formation of cement-like glue,⁴ aquaplastics⁵ or three-dimensional (3D)-printed living materials.^{6,7} The composition of the biofilm matrix and the interaction between the matrix components critically determine its mechanical properties. The matrix mainly consists of polysaccharides,⁸ proteins,⁹ and nucleic acids.¹⁰ The type of protein and polysaccharide as well as their proportion vary remarkably, both between genera and between different species within the same genus.¹¹ Protein-based amyloid fibers are particularly widespread in microbial biofilms and were, for example, observed in *Pseudomonas* sp., *Bacillus* sp. and *Escherichia coli* biofilms, where they are referred to as curli fibers.¹² Curli fibers, encoded by the *csgBA* operon, are composed of several CsgA units that polymerize onto the CsgB nucleator protein.¹³ The second main component of *E. coli* biofilms is phosphoethanolamine-modified cellulose

(pEtN-cellulose).¹⁴ The matrix of the biofilm-forming *E. coli* K-12 strain AR3110 was estimated to contain 75% curli and 25% pEtN-cellulose.¹⁵

In addition to the matrix composition, also environmental factors influence the mechanical properties of biofilms. For instance, substrate water content, temperature, pH, and nutrients may be utilized as possible control parameters for tuning *E. coli* biofilm properties.^{16,17} Another possible parameter is the addition of specific metal ions. Metal ions frequently bind to protein or carbohydrate structures in biological materials,¹⁸ forming either mineralized composite materials^{19–22} or sacrificial and self-healing bonds.^{23,24} Bacterial biofilms frequently occur in metallic pipes or at the surface of heavy metal-containing wastewaters, suggesting a possible influence of metal ions on biofilm growth and properties. For *Enterobacter asburiae*, *Vitreoscilla* sp., and

Received: October 5, 2022

Accepted: January 19, 2023

Published: January 27, 2023



Acinetobacter lwoffii, metal ions promote biofilm formation.²⁵ In the case of *Staphylococcus epidermidis*, *Bacillus subtilis*, and *Pseudomonas aeruginosa*, biofilms stiffen in the presence of metal cations.²⁶ Specifically, *B. subtilis* biofilms stiffen and erode more slowly in the presence of Fe(III) and Cu(II).²⁷

In the present work, we focused on *E. coli* biofilms and investigated their viscoelastic properties in the absence and presence of the bivalent metal cations Zn(II) and Ca(II) as well as the trivalent cations Al(III) and Fe(III). Performing shear rheology, we compared homogenized biofilm samples where a solution of a specific metal cation was added and samples where the same volume of water was added as a control. We further compared the *E. coli* K-12 strain AR3110, which produces biofilms with curli and pEtN-cellulose, with two closely related strains that synthesize either curli or pEtN-cellulose fibers.^{14,28} Only biofilms that contain both matrix fibers stiffen when incubated with trivalent metal ions. When strains that produce only curli or pEtN-cellulose are co-cultured or simply mixed, no cation-induced stiffening is observed, indicating that both matrix fibers need to be produced from the same bacterial cell. These results suggest the formation of a composite material during matrix production.

MATERIALS AND METHODS

Bacterial Strains. Three different *E. coli* strains were used to distinguish between the contributions of the two main matrix fibers to the mechanical biofilm properties and the dependence of these properties on the presence of metal cations. W3110 is a non-pathogenic K-12 strain²⁹ that produces curli amyloid fibers and lacks the ability to synthesize cellulose. Cellulose synthesis, which is encoded in the *bcs* operon, was restored in the strain AR3110.²⁸ This W3110-based strain thus produces both curli amyloid fibers and pEtN-cellulose. To obtain a strain that produces only pEtN-cellulose, curli production was inactivated in the strain AP329.¹⁴ To test biofilm properties when both curli and pEtN cellulose are present, but not produced by the same bacterial cell, W3110 and AP329 were combined before inoculation (co-seeded) or when harvesting the mature biofilms for the rheology experiments (mixed).

Metal Solutions. The following salts were used to probe the influence of trivalent and bivalent cations on biofilm properties: aluminum chloride hexahydrate (97%; 26726139, Molekula GmbH), iron(III) chloride anhydrous (1/1035/50, Fisher Scientific), zinc chloride ($\geq 98\%$) (29156.231, VWR International), calcium chloride dihydrate ($\geq 99\%$; C3306, Sigma-Aldrich). AlCl₃, FeCl₃, ZnCl₂, and CaCl₂ were dissolved in ultrapure water to a concentration of 220 mM, and the pH was measured with a pH-meter (WTW GmbH; Table 1). Using the FeCl₃ solution as a reference, a control solution with an identical pH was prepared with hydrochloric acid (1.09057, Merck KGaA). In addition to the pH, the osmolality of the

metal solutions can also influence biofilm properties via water intake of the biofilm. The osmolalities of the different solutions were measured with an osmometer (Osmomat 3000, Gonotec GmbH). The osmolalities were determined from a calibration curve established from solutions of sodium chloride (39781.02, Serva Electrophoresis) (Table 1 and Figure S1). Similar to the pH control, a NaCl solution was prepared that matched the osmolality of the FeCl₃ solution.

Biofilm Growth. For starting the bacterial culture, LB agar plates (Luria/Miller; x969.1, Carl Roth GmbH) were prepared. A bacterial suspension, grown from glycerol stocks, was streaked onto these agar plates to obtain microcolonies after overnight culture at 37 °C. One day before starting biofilm growth, two single microcolonies were separately transferred into the LB medium (5 mL; Luria/Miller; x968.2, Carl Roth GmbH) and incubated overnight at 250 rpm and 37 °C. The OD₆₀₀ of the resulting bacteria suspensions was measured after a 10-fold dilution. The suspension where the OD₆₀₀ of the diluted sample was closest to 0.5 was chosen for inoculating the biofilms. Biofilms were grown on salt-free LB agar plates as media with low osmolarity promote matrix production.³⁰ The salt-free LB agar plates were composed of tryptone/peptone ex casein (10 g L⁻¹; 8952.1, Carl Roth GmbH), yeast extract (5 g L⁻¹; 2363.1, Carl Roth GmbH), and bacteriological agar agar (18 g L⁻¹; 2266.3, Carl Roth GmbH). On each Petri dish ($\phi = 145$ mm), $9 \times 5 \mu\text{L}$ of the undiluted suspension was inoculated to obtain an array of nine biofilms. For the “co-seeded” biofilm samples, OD₆₀₀ of the two suspensions was measured and the suspensions were combined such that the final density of each bacterial strain was identical. Inoculation took place immediately after a short mixing step. For the “mixed” samples, both bacterial strains were grown on the same agar surface. All biofilms were grown at 28 °C for 7 days and then stored in the fridge at 5 °C for a maximum of 48 h. Images of the biofilms were acquired using an AxioZoomV.16 stereomicroscope (Zeiss, Germany).

Sample Preparation for Rheology Experiments. Depending on the *E. coli* strain, two or three biofilms (~90 mg) were scraped from the agar surface and transferred into an empty Petri dish using cell scrapers. For the “mixed” biofilm samples, materials from both strains were combined in equal proportions. All samples were gently stirred with a pipette tip and either measured as obtained (neat) or incubated with the desired metal or control solution (diluted). For the experiments that required the incubation of the biofilm with the respective solution, the scraped biofilms were stirred with the solution in a ratio of 10:1 (w/v), yielding a final cation concentration of ~20 mM. After stirring, the Petri dish was sealed with Parafilm and left to incubate at room temperature for 45 min. For every dilution experiment, two samples from the same agar plate were measured. One was incubated with the solution of interest and the other sample was incubated with ultrapure water. To document the sample texture, images of the different mixtures were taken using a 2 megapixel USB camera (Toolcraft Microscope Camera Digimicro 2.0 Scale, Conrad Electronic SE).

Rheology Measurements. The measurements were performed using an oscillatory shear rheometer (MCR301, Anton Paar GmbH) under stress control. The sample stage was equipped with Peltier thermoelectric cooling and the temperature was set to 21 °C for all measurements. Once the sample was transferred onto the stage, a channel around the stage was filled with water and a hood was used to maintain a

Table 1. Concentration, pH, and Osmolality of the Four Metal Solutions FeCl₃, AlCl₃, ZnCl₂, and CaCl₂ and the NaCl and HCl Control Solutions

solution	AlCl ₃	FeCl ₃	ZnCl ₂	CaCl ₂	NaCl	HCl
concentration (mM)	220	220	220	220	409	32
pH	2.8	1.5	5.7	5.2		1.5
osmolality (mOsmol/kg)	895	754	598	618	754	

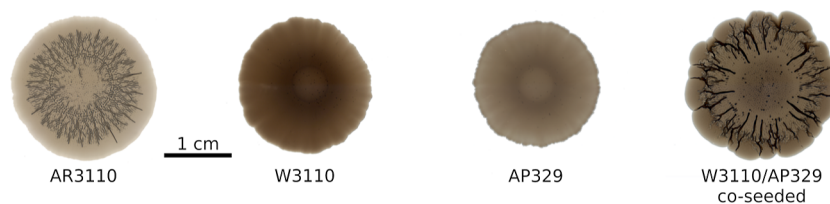


Figure 1. Phenotypes of the different *E. coli* strains. AR3110 produces both curli fibers and pEtN-cellulose. W3110 expresses only curli, while AP329 synthesizes only pEtN-cellulose. The sample W3110/AP329 shows the biofilm morphology obtained when W3110 and AP329 were co-seeded, i.e., when curli and pEtN-cellulose were produced by different bacteria. (W3110/AP329 co-seeded photograph courtesy of Ricardo Ziege. Copyright 2023.)

high humidity environment. A parallel plate geometry ($\phi = 12$ mm) was used and the gap was set to $250 \mu\text{m}$.

To quantify the viscoelastic properties of the biofilm, strain amplitude sweeps were carried out to determine the linear viscoelastic range (LVE) and to extract the storage (G_0') and loss (G_0'') moduli. The oscillation frequency was set to 10 rad s^{-1} . The strain amplitude was increased from 0.01 to 100% with 7 points per decade and then decreased again. These cycles of ascending and descending strain amplitude were repeated 3 \times . One experiment with three cycles lasted approximately 45 min. The data presented in the Results section were extracted from the ascending amplitude sweep in the second cycle. The first cycle was considered as an additional homogenization step.

To validate the chosen oscillation frequency, frequency sweeps were performed for AR3110 samples. The strain amplitude was set constant to 0.02%. The oscillation frequency was decreased step-wise from 100 to 1 rad s^{-1} with 7 points per decade. Alternatively, frequency sweeps were also performed with a frequency increasing from 1 to 100 rad s^{-1} . This ranged from 1 order of magnitude above and below the frequency used for the amplitude sweeps. Frequency sweeps were also performed over a wider range of frequencies, i.e., from 100 to 0.001 rad s^{-1} ; however, these measurements showed excessive drying of the biofilm samples at low frequencies. All frequency sweeps were carried out with neat biofilms and samples mixed with 10% (v/w) ultrapure water and both preceded or not by a pair of increasing and decreasing amplitude sweeps as previously described.

To validate that sample drying does not affect the data acquired within the second ascending amplitude sweep, sample properties of AR3110 were recorded for a duration of at least 3 h using a low oscillation frequency of 10 rad s^{-1} and strain amplitude of 0.02%. This test was also preceded by a pair of amplitude sweeps (increasing and decreasing strain amplitude) as previously described.

Data Analysis. To determine biofilm properties, the G' and G'' values were averaged over a strain range from 0.01 to 0.02% (3 data points). These values represent the plateau moduli G_0' and G_0'' of the respective biofilms (neat samples vs samples diluted with ultrapure water). For the dilution experiments with solutions of metal cations, we primarily focused on the relative difference between moduli. That is, the modulus of the sample diluted with the solution of interest was corrected by the modulus of a sample (from the same Petri dish) diluted with ultrapure water. This comparison to a reference sample grown under identical conditions, was necessary to account for biofilm sample variability between Petri dishes.

For both moduli, the relative difference was calculated as follows, as exemplarily shown for G_0'

$$\Delta G_0' = \frac{G_{0,\text{solution}}' - G_{0,\text{water}}'}{G_{0,\text{water}}'}$$

For each condition tested, the median was determined ($n_{\text{pairs}} \geq 4$) as the data were not normally distributed. The data are shown in the form of boxplots. The whiskers of the boxplots represent 1.5 times the interquartile range (IQR). To assess whether the relative differences of the moduli show a significant difference from zero, i.e., the effect of the solution tested differs from that of water, a one-sample Wilcoxon signed rank test ($\mu = 0$, $\alpha = 0.05$) was performed using the program R (R Core Team; version 4.0.5).

RESULTS

Biofilms that synthesize both curli and pEtN-cellulose (AR3110) showed the typical morphology with 3D wrinkles (Figure 1).¹⁴ In contrast, the strains producing only curli (W3110) or pEtN-cellulose (AP329) showed different morphologies in agreement with the literature.^{14,28} When co-seeding W3110 and AP329, the biofilm morphology was similar to that of AR3110, suggesting that the structural and mechanical properties of the matrix are at least partly restored in the co-seeded biofilm.

For measuring the viscoelastic properties, the biofilms were harvested and mildly homogenized by stirring. It has previously been suggested that homogenized *P. aeruginosa* biofilms quickly regain their viscoelastic properties when probed with shear rheology.³¹ Here, homogenization was necessary to mix the harvested biofilms with the metal cation solution of interest. As trivalent metal ions, Al(III) and Fe(III) were chosen for their known effects on the viscoelastic properties of *B. subtilis* and *P. aeruginosa* biofilms. Fe(III) has coordination numbers ranging from 4 to 6,³² Al(III) has 4 and 6, rarely 5.³³ Zn(II) and Ca(II) were chosen as two bivalent cations with different preferred coordination numbers [Zn(II): 4–6, Ca(II): 6–8].^{32,34}

Selection of Measurement Conditions and Data Range for Rheology Analyses. Before probing the influence of bivalent and trivalent cations on the mechanical properties of the different biofilms, we first established the measurement conditions using neat AR3110 biofilms. As previously stated, the amplitude sweeps consisted of three cycles, and the data presented were extracted from the ascending amplitude sweep in the second cycle (Figure 2A). The plateau values for both moduli were similar for the three cycles, with no systematic increase or decrease of the values between the first and subsequent cycles (Figure S2). This confirms that also homogenized *E. coli* biofilms recover their stiffness within a few minutes after yielding, similarly to what was observed for *P. aeruginosa*.³¹

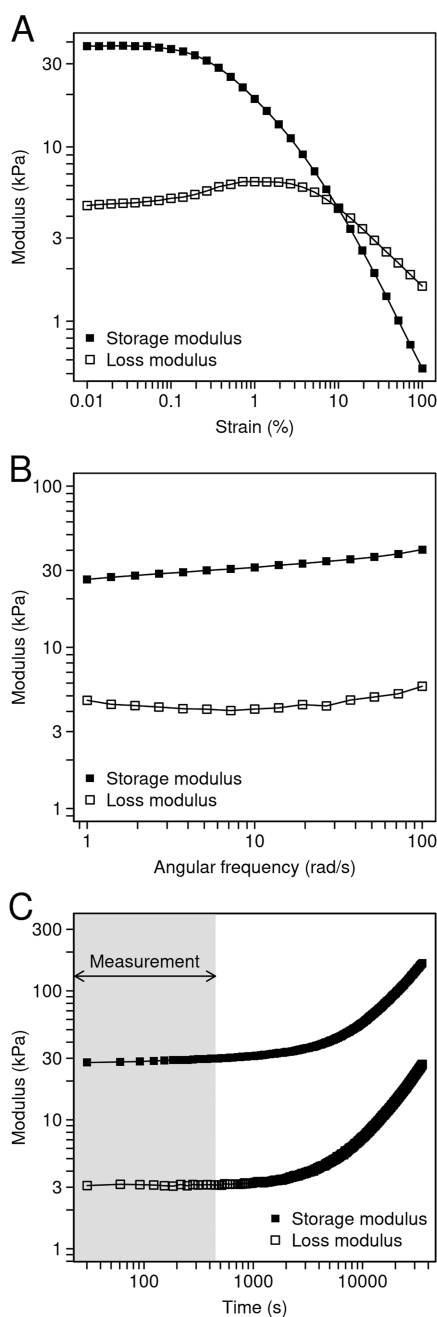


Figure 2. Viscoelastic properties of AR3110 biofilms producing both matrix fibers. (A) Strain amplitude sweep ($\omega = 10 \text{ rad s}^{-1}$) of a biofilm where no solution was added. (B) Frequency sweep ($\gamma = 0.02\%$, decreasing frequency) of a biofilm where no solution was added. (C) Evolution of the storage and loss moduli measured with a constant strain amplitude ($\gamma = 0.02\%$) and frequency ($\omega = 10 \text{ rad s}^{-1}$). The biofilms were measured without any solution added, and the measurement was preceded by one amplitude sweep (not shown). The time interval of the analyzed ascending amplitude sweep (7.5 min) is labeled in gray.

To assess the validity of the strain amplitude sweeps, frequency sweeps were performed. The storage and loss moduli showed a limited influence of the oscillation frequency over a range from 1 to 100 rad s^{-1} (Figure 2B). Similar viscoelastic properties were observed for frequency sweeps with increasing and decreasing frequency and for samples with and without the addition of 10% (v/w) ultrapure water (Figure

S3). Consequently, in the amplitude sweeps, the plateau moduli G_0' and G_0'' were always obtained from the LVE range (Figure 2A) at a frequency of 10 rad s^{-1} . Frequencies below 1 rad s^{-1} were also tested, but the sample showed a strong increase in the values of both moduli, supposedly due to sample drying (Figure S4).

The effect of drying was subsequently investigated in more detail. We focused on the time window of the second ascending amplitude sweep from which the shear moduli were derived. Although the sample appears to be continuously drying throughout the experiment, the drying effect accounts for only 10% of the increase in G_0' during this period (Figure 2C). Interestingly, the values for both moduli ($G_0' \approx 30 \text{ kPa}$ and $G_0'' \approx 3 \text{ kPa}$) are significantly lower than those measured for the *E. coli* strain MG1655 ($G_0' \approx 100 \text{ kPa}$ and $G_0'' \approx 20 \text{ kPa}$), which produces a matrix with a different composition (curli and PGA, a linear polymer of β -1,6-*N*-acetyl-D-glucosamine).³⁵

Dispersion of the Storage and Loss Moduli upon Dilution. Adding metal ions in solutions increases the water content of the biofilm–cation mixture. Changes in biofilm properties are thus a combined effect from the addition of water and from the respective metal ion. To disentangle these effects, we first investigated changes in biofilm viscoelasticity in response to the addition of 10% (v/w) ultrapure water. In general, both storage and loss moduli decreased by approximately 1 order of magnitude. For example, for AR3110 biofilms, the storage modulus decreased from 30 to 4 kPa (Table 2) and the loss modulus was lowered from 3 to 0.4 kPa (Table 3). This indicates that the architecture of the biofilm matrix is partially destroyed when the sample is stirred after the addition of water. This observation relates to results obtained in *P. aeruginosa* biofilms where the addition of 5% (v/w) water led to a stiffness decrease of 40%.³¹ In most cases, the addition of water also increased the dispersion (coefficient of variation) in both moduli (Tables 2, 3, S1 and S2). Considering the overall large dispersion between biofilm samples grown on different days and as a result of stirring, the following measurements to probe the effect of metal ions were performed with an internal control. Each metal-containing sample was compared to a sample containing 10% (v/w) ultrapure water that was grown in the same Petri dish (Figure 3A; Materials and Methods).

Effect of Trivalent Cations on the Shear Modulus of AR3110 Biofilms. To address the great variability between samples grown on different Petri dishes, bacteria were always seeded such that biofilm material sufficient for two samples could be obtained from the same Petri dish. After 1 week of growth, the biofilms were scraped from the agar. Prior to the rheology measurements, one sample was incubated with ultrapure water, while the other one was incubated with the solution of interest. This allowed a systematic comparison dish per dish between the samples incubated with a metal solution and the respective control samples incubated with water (Figure 3A).

Immediately following the addition of the metal ion solutions to AR3110 biofilms, the mixtures showed a striking difference in their visual appearance (Figure 3B). The texture of biofilms containing AlCl_3 or FeCl_3 was similar to a granular paste. In contrast, the biofilm mixture appeared more fluid and smooth when ZnCl_2 or CaCl_2 was added. No such difference between bivalent and trivalent cations was observed for any other matrix composition.

Table 2. Median Storage Moduli (G_0') before (–) and after (+) Dilution of the Biofilms with 10% (v/w) Ultrapure Water ($n_{\text{experiments}} \geq 3$)^a

matrix composition	curli + pEtN-cellulose		curli		curli + pEtN-cellulose (mixed)		curli/pEtN-cellulose (mixed)		curli + pEtN-cellulose (co-seeded)	
	–	+	–	+	–	+	–	+	–	+
water										
median G_0' (Pa)	28267	4510	16533	1580	18200	576	31267	2673	51167	5617
median absolute deviation (Pa)	4567	863	6517	367	9043	385	4267	1250	3233	2717
coefficient of variation (MAD/median) (%)	16	19	39	23	50	67	14	47	6	48

^aThe G_0' values of all individual experiments are reported in Table S1.

Table 3. Median Loss Moduli (G_0'') before (–) and after (+) Dilution of the Biofilms with 10% (v/w) Ultrapure Water ($n_{\text{experiments}} \geq 3$)^a

matrix composition	curli + pEtN-cellulose		curli		pEtN-cellulose		curli + pEtN-cellulose (mixed)		curli + pEtN-cellulose (co-seeded)	
	–	+	–	+	–	+	–	+	–	+
water										
median G_0'' (Pa)	3297	442	2047	170	2187	61	3413	225	6390	695
median absolute deviation (Pa)	1033	83	657	14	1007	46	277	91	160	149
coefficient of variation (MAD/median) (%)	31	19	32	8	46	75	8	40	3	21

^aThe G_0'' values of all individual experiments are reported in Table S2.

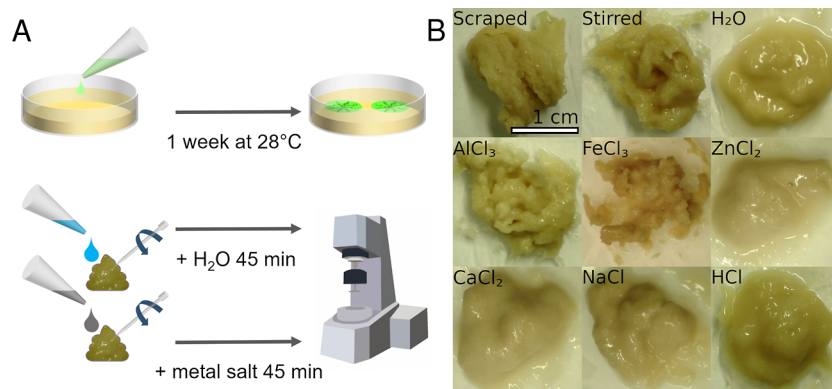


Figure 3. Sample preparation and texture. (A) Biofilms were inoculated on salt-free LB agar and grown for 1 week at 28 °C. One Petri dish contained material for two rheology experiments. After harvesting two samples of the biofilm material, the metal solution of interest was added to one sample and the sample was gently stirred with a pipette tip. Ultrapure water was added to the second sample, which was then treated in the same way. Both samples were incubated for 45 min, followed by the rheology measurements. (B) Texture of AR3110 biofilm material after stirring with various solutions. Biofilms stirred with ultrapure water (H_2O), with the control solutions or solutions with bivalent metal cations appear more liquid. In contrast, the samples containing trivalent metal ions show a more solid textural appearance.

To quantify the observed texture changes, G_0' and G_0'' were determined for all different biofilm samples incubated with the different metal ion solutions or the control solutions. Consistent with the changes in texture, the moduli also differed when the AR3110 biofilms were mixed with bivalent or trivalent metal cations. The addition of $AlCl_3$ or $FeCl_3$ increased the storage and loss moduli for AR3110 (Figure 4). Neither did the bivalent metal ions cause an increase in either modulus nor did the control solutions that mimicked the pH value or osmolality of the $FeCl_3$ solution (Figure 4).

Although statistically significant (Tables 4 and 5), the increase in stiffness (G_0') was smaller than what was observed for other bacteria species. For example, Fe(III) and Al(III) led to a 100-fold increase of the storage modulus of *P. aeruginosa* biofilms.³¹ Moreover, a range of bivalent and trivalent metal cations increased the storage modulus of *B. subtilis* biofilms by several orders of magnitude. Such discrepancies in the magnitude of the observed stiffening might be due to the differences in sample preparation and in matrix composition.

Indeed, in the case of *P. aeruginosa*, only 5% (v/w) solution was added,³¹ i.e., less than in our case (10%). In *B. subtilis*, the final metal concentration in the biofilm was 0.25 M,³⁶ whereas it was 0.02 M in our case. Moreover, the biofilm matrix of the *P. aeruginosa* PAO1 strain contains at least three polysaccharides (alginate, Psl, and Pel),³⁷ and the *B. subtilis* B-1 strain produces mainly γ -polyglutamate, which both differ from the curli and pEtN-cellulose found in the *E. coli* biofilm matrix.

The effect induced by Fe(III) also depends on the matrix composition (Figure 4). While the ferric salt caused a stiffening of the biofilm sample containing curli and pEtN-cellulose fibers (+50% in G_0'), it caused a softening (–50% in G_0') for the matrix composed of curli fibers only and no statistically significant effect for the matrix composed of pEtN-cellulose. The effect remained unclear for the co-seeded and mixed biofilms. The bivalent ions caused a significant decrease (>50%) in G_0' for the matrices containing only one type of fiber (Figure 4), while no such effect was observed for the AR3110 strain producing both fibers. One possible explanation

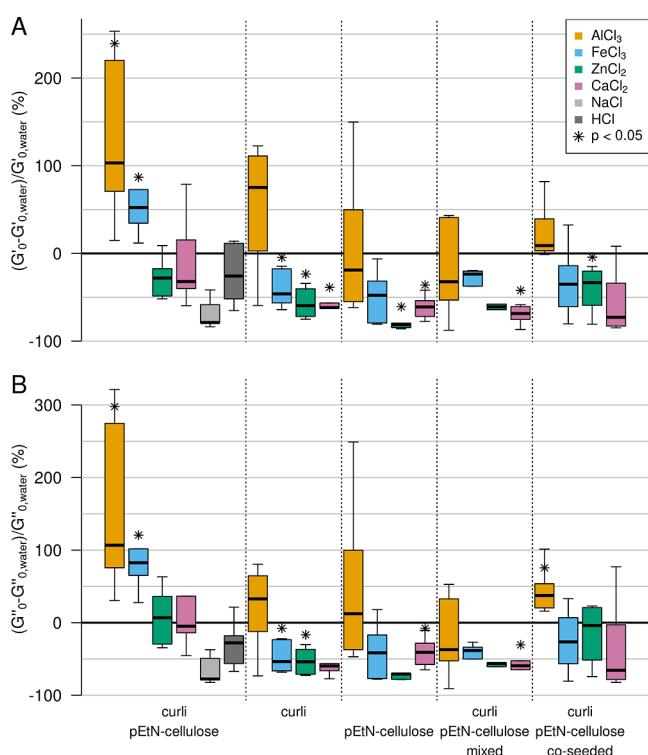


Figure 4. Effect of bivalent and trivalent metal ions on *E. coli* biofilms with different matrix compositions. (A) Storage moduli. (B) Loss moduli. All samples were stirred with the respective metal cation or control solution, adding 10% (v/w) of the respective solution. The boxplots highlight the median of ≥ 4 independent experiments (see Tables S3–S12 for all values). The whiskers represent 1.5 times the IQR.

for the decrease in stiffness observed for most matrix–metal combinations is a non-specific osmotic effect caused by the addition of the ionic solution. The Fe(III)- and Al(III)-induced net stiffening of the AR3110 matrix overrules this softening observed in all other samples. This suggests that the curli and pEtN cellulose fibers co-produced by AR3110 bacteria form a composite material with a built-in response to trivalent ions.

DISCUSSION

Using shear rheology, we examined how the viscoelastic properties of *E. coli* biofilms vary under the influence of metal cations. We probed biofilms formed by different *E. coli* strains that produce pEtN-cellulose and/or curli fibers. While the shear modulus generally decreased in the presence of metal solutions, it specifically increased when trivalent cations were

added to a biofilm made from bacteria that co-produced both fibers. Metal cations trigger the formation of biofilms in *E. asburiae*, *Vitreoscilla* sp., and *A. lwoffii*.²⁵ Moreover, biofilms produced by *B. subtilis*, *Pseudomonas putida*, and *Shewanella oneidensis* allow for the biosorption of metal ions.³⁸ In *E. coli* biofilms, the greatest biosorption performance was observed for Fe(III) when compared to Cd(II), Ni(II), or Cr(VI), but biofilm mechanical properties were not investigated.³⁹ In other species, changes in mechanical biofilm properties were observed,²⁶ revealing that the same ion can have opposite effects in different bacterial species. While Cu(II) reinforces *B. subtilis* B-1 biofilms, it weakens those produced by *P. aeruginosa*.^{31,36} This suggests a specific interplay between the matrix composition and the type of ion. In a strain of *B. subtilis* producing a multi-component matrix, however, the effect of metal cations on the biofilm viscoelastic properties did not seem to be dictated by any specific matrix component.²⁷

To interpret the present results, a molecular understanding of the possible interaction of trivalent cations with the matrix fibers is required. To our knowledge, no data are available concerning the interaction of Al(III) or Fe(III) with pEtN-cellulose. However, it was demonstrated that phosphorylation of cellulose nanofibers significantly enhances their adsorption capacity of Fe(III) ions.⁴⁰ Most interestingly, phosphorylated bacterial cellulose has a much stronger affinity for Fe(III) ions than for Zn(II), in particular in acidic solutions.⁴¹ It was also shown that Fe(III) ions exhibit a tetrahedral coordination when bound to hydroxyethyl cellulose or carboxymethyl cellulose.⁴² Tetrahedral coordination is the second most common geometry for Fe(III) after octahedral, but it is also the most common coordination geometry for Zn(II).³² This may suggest that the overall charge is more important than the coordination geometry. This charge specificity could be explained by counter ion condensation, a phenomenon where ions condense along a polyionic chain of opposite charge, reducing the charge density along the chain. This can in turn lead to changes in chain conformation, their interaction with other polymers, and therefore affect the viscoelastic properties of the biofilm.³⁶ Ion condensation occurs when Manning's criterion is satisfied (see the Supporting Information).^{51,52} According to our calculations, counter ion condensation can take place along the pEtN-cellulose chain in the presence of both bivalent and trivalent cations, while it is probably stronger for the trivalent ions.

Equally little information is available about the interaction between metal cations and amyloid curli fibers. It was demonstrated that curli fibers sequester Hg(II) ions, suggesting a possible general ability to bind metal cations.⁴³ More broadly, the interaction between metal cations and other

Table 4. Statistical Significance between the Effect of a Metal Solution on the Storage Modulus (G') and the Effect of Water⁴⁴

matrix composition	curli + pEtN-cellulose	curli	pEtN-cellulose	curli + pEtN-cellulose (mixed)	curli + pEtN-cellulose (co-seeded)
AlCl ₃	↑0.001	0.094	0.844	0.563	0.063
FeCl ₃	↑0.031	↓0.031	0.063	0.063	0.156
ZnCl ₂	0.063	↓0.031	↓0.031	0.063	↓0.031
CaCl ₂	0.563	↓0.031	↓0.031	↓0.031	0.063
NaCl	0.063				
HCl	0.313				

⁴⁴Shown are the p -values calculated from a one-sample Wilcoxon signed rank test ($\mu = 0$) assessing the effect of one solution on G' for each matrix composition. H_0 : the variation of G' does not differ significantly from zero. p -Values inferior to 0.05 are in bold, in which case an arrow indicates whether the modulus increases (↑) or decreases (↓).

Table 5. Statistical Significance between the Effect of a Solution on the Loss Modulus (G'') and the Effect of Water^a

matrix composition	curli + pEtN-cellulose	curli	pEtN-cellulose	curli + pEtN-cellulose (mixed)	curli + pEtN-cellulose(co-seeded)
AlCl ₃	↑0.001	0.563	0.447	0.563	↑0.031
FeCl ₃	↑0.031	↓0.031	0.188	0.063	0.313
ZnCl ₂	0.563	↓0.031	0.063	0.063	0.563
CaCl ₂	1	0.063	↓0.031	↓0.031	0.219
NaCl	0.063				
HCl	0.188				

^aShown are the p -values calculated from a one-sample Wilcoxon signed rank test ($\mu = 0$) assessing the effect of one solution on G'' for each matrix composition. H_0 : the variation of G'' does not differ significantly from zero. p -Values inferior to 0.05 are in bold, in which case an arrow indicates whether the modulus increases (\uparrow) or decreases (\downarrow).

amyloid-forming structures was widely investigated. This includes amyloid beta ($A\beta$) peptides, which are the main components of amyloid plaques responsible for Alzheimer's disease. While Fe(III), Al(III), and Zn(II) co-localize with $A\beta$ in senile plaques, their influence on the *in vitro* formation of amyloid fibrils differs. Zn(II) inhibits the formation of β -sheets, while trivalent cations both trigger and stabilize them.⁴⁴ 3D-models have shown that Al(III) is almost always hexacoordinated and interacts with aspartate and glutamate residues in $A\beta$ -complexes.⁴⁵ Zn(II) coordinates four to six ligands in $A\beta$ -complexes, including three histidines as well as one aspartate and/or glutamate residue.⁴⁶ Although there is a lack of structural studies on Fe(III)-coordination to $A\beta$,⁴⁷ ferric ions bind histidine more efficiently than Zn(II).⁴⁸ A 3D-structure prediction of the major curlin subunit CsgA (AlphaFold; Figure 5) reveals the close proximity of several surface-exposed histidine, glutamate, and aspartate residues, suggesting that several residues are available for metal coordination.^{49,50}

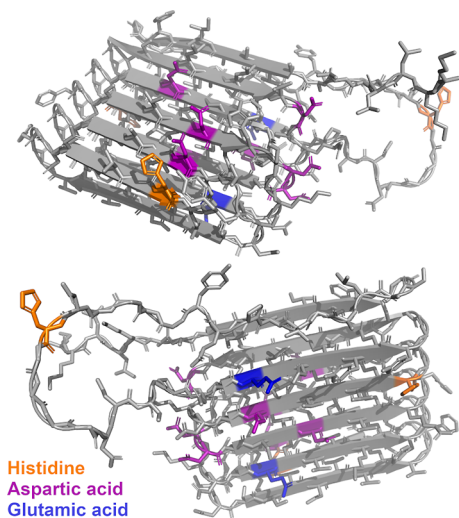


Figure 5. Tertiary structure of CsgA, the major curlin subunit, as predicted by AlphaFold (top and bottom views). Amino acids known to be involved in metal coordination are highlighted as follows: orange—histidine, purple—aspartic acid, and blue—glutamic acid.

Our results indicate that the stiffening effect observed for the strain producing both pEtN-cellulose and curli amyloid fibers does not take place in co-seeded biofilms where each strain produces one type of fiber (Figure 4, Tables 4 and 5). We assumed that the total amount of each fiber would be similar in the strain producing both or only one type of fiber. Combining them in equal proportions would then yield the original ratio between the two fibers, i.e., 75% curli and 25% pEtN-

cellulose,¹⁵ although with a lower total concentration. However, strains producing only one type of fiber could potentially dedicate more energy to the production of the respective fiber than the strain producing both. Co-seeding biofilms with different ratios of curli- and pEtN-cellulose-producing strains may eventually result in a better reconstitution of the original matrix composition. At the same time, a spatial segregation of the two bacterial populations is expected, as observed for *B. subtilis*⁵³ as well as for biofilms of two competing *E. coli* strains.⁵⁴ In such a scenario, the two fibers do not co-localize and interact only at the interface between clusters of different bacteria populations. Intriguingly, co-seeding of the curli- and pEtN-cellulose-producing strains partially restores the phenotype of the strain producing both fibers (Figure 1). Further work will be needed to clarify the determinants of strain segregation and/or matrix fiber interactions in biofilms grown from mixed bacterial suspensions.

While our results point toward a determining role of the matrix, they do not allow us to exclude a possible effect of the metal ions on the bacteria themselves. Since metal ions trigger biofilm formation in various species,²⁵ matrix production may be regulated by the presence of metal ions. Considering the timescale of our experiments, altered expression of matrix components is considered to play a minor role, however. Bacteria may further respond to reduce a possible toxic effect of heavy metal ions. For planktonic *E. coli* cells, it was shown that Fe(III) and Al(III) in a concentration of 0.01 mM reduce the number of colony forming units by 50%.⁵⁵ While it appears likely that biofilms provide protection against heavy metal toxicity, as demonstrated for *P. aeruginosa*,⁵⁶ it cannot be fully neglected that these cations also have an effect on *E. coli* cells in biofilms. It is reasonable to assume, however, that the viscoelastic biofilm properties are not significantly altered by the appearance of non-viable bacteria as bacterial cells can most likely be considered as particles in a composite material. Most importantly, toxicity would affect all strains equally, while we observe a clear difference between strains producing different matrix fibers. Similar to the condensation discussed at the fiber scale, aggregation of the negatively charged bacteria via neutralization by metal cations is also to be considered. In *E. coli* suspensions monitored with dynamic light scattering, 10 μ M Fe(III) or Al(III) showed little to no effect on cell size distribution. Thus, if these ions caused aggregation, the formed aggregates are still small.⁵⁵ Here, the metal ion concentrations in the biofilms were much higher (20 mM), and cell aggregation induced by trivalent cations may occur in the biofilms. However, this effect would occur equally for all matrix compositions so that differences between strains must originate from other factors than ion-induced cell aggregation.

Osmolarity may also play a role as *E. coli* K-12 were shown to rapidly adapt (within a few minutes) to increases in osmolarity. By uptake of potassium ions, they maintain an internal osmotic pressure higher than that of the environment, which is necessary for growth.⁵⁷ After 45 min of incubation, however, an osmolarity-triggered shrinking of bacteria is no longer expected to impact biofilm mechanics. Considering biofilms as complex hydrogels, they could potentially swell at higher osmotic pressures. This would in turn affect their viscoelastic properties.⁵⁸ Swelling could partially explain the non-specific decrease in stiffness observed upon exposure to most solutions (Figure 4). However, the magnitude of the decrease (as far as -50% in G_0') is hardly compatible with the little amount of water added (i.e., about 10% in volume). In general, not all biofilms have reached a swelling equilibrium as excess water is observed around biofilms mixed with bivalent ion solutions but not with trivalent solutions (Figure 3). The complexity of biofilm materials, together with these swelling differences, prohibits a quantitative assessment of the impact of osmotic pressure changes on biofilm stiffness.

CONCLUSIONS

Investigating the influence of Fe(III), Al(III), Zn(II), and Ca(II) on the viscoelastic properties of *E. coli* biofilms, we observed a slight stiffening in the presence of trivalent cations. This stiffening only occurred for the strain that produced a matrix composed of both pEtN-cellulose and curli amyloid fibers. Derivatives of bacterial cellulose as well as amyloid-forming structures are known to bind metal cations; however, no molecular level information is currently available about the interaction of *E. coli*-produced pEtN-cellulose and curli fibers. Considering that stiffening only occurs when both fibers are co-produced by one and the same bacterial cell, it is highly likely that the trivalent cations simultaneously interact with both components. Further research is required to unravel the molecular interactions that underlie this highly selective and specific biofilm stiffening. Toward this goal, experiments with purified and/or synthetic matrix components may provide mechanistic insights into the cation–matrix interaction. These experiments will further allow for probing the role of the phosphoethanolamine modification. Ultimately, the present work and the proposed follow-up studies will pave the way for new strategies to control biofilm viscoelastic properties without the need for genetic engineering, a topic of interest for both biofilm prevention and biofilm-based materials engineering.

ASSOCIATED CONTENT

Supporting Information

The Supporting Information is available free of charge at <https://pubs.acs.org/doi/10.1021/acsomega.2c06438>.

Osmolality measurement; amplitude sweeps for AR3110 samples with ascending and descending strain amplitude; frequency sweeps for AR3110 samples prepared under different conditions; effect of diluting biofilm samples with ultrapure water; dilution experiments with metal cation solutions; and counter ion condensation (PDF)

AUTHOR INFORMATION

Corresponding Authors

Kerstin G. Blank – *Mechano(bio)chemistry, Max Planck Institute of Colloids and Interfaces, 14476 Potsdam,*

Germany; Institute of Experimental Physics, Johannes Kepler University, 4040 Linz, Austria; orcid.org/0000-0001-5410-6984; Email: kerstin.blank@jku.at

Cécile M. Bidan – *Department of Biomaterials, Max Planck Institute of Colloids and Interfaces, 14476 Potsdam, Germany; orcid.org/0000-0002-6243-562X; Email: cecile.bidan@mpikg.mpg.de*

Authors

Adrien Sarlet – *Department of Biomaterials, Max Planck Institute of Colloids and Interfaces, 14476 Potsdam, Germany*

Valentin Ruffine – *Mechano(bio)chemistry, Max Planck Institute of Colloids and Interfaces, 14476 Potsdam, Germany*

Complete contact information is available at: <https://pubs.acs.org/10.1021/acsomega.2c06438>

Funding

Open access funded by Max Planck Society.

Notes

The authors declare no competing financial interest.

ACKNOWLEDGMENTS

The authors thank Regine Hengge and Diego O. Serra for kindly providing the *E. coli* strains used in this work, Christine Pilz-Allen and Reinhild Dünnebacke for technical support in the laboratories, Angelo Valleriani for help with statistics, Geonho Song with rheology, Ricardo Ziege with microscopy, and Wenbo Zhang with osmometry. They further thank the International Max Planck Research School (IMPRS) on Multi-Scale Biosystems for funding and support as well as Peter Fratzl and the members of the Biofilm-based Materials and the Mechano(bio)chemistry research groups (Max Planck Institute of Colloids and Interfaces) for inspiring discussions.

REFERENCES

- (1) Reisner, A.; Maierl, M.; Jorger, M.; Krause, R.; Berger, D.; Haid, A.; Tesic, D.; Zechner, E. L. Type 1 Fimbriae Contribute to Catheter-Associated Urinary Tract Infections Caused by *Escherichia Coli*. *J. Bacteriol.* **2014**, *196*, 931–939.
- (2) Shemesh, M.; Ostrov, I. Role of *Bacillus* Species in Biofilm Persistence and Emerging Antibiofilm Strategies in the Dairy Industry. *J. Sci. Food Agric.* **2020**, *100*, 2327–2336.
- (3) Zhang, L.; Keller, J.; Yuan, Z. Inhibition of Sulfate-Reducing and Methanogenic Activities of Anaerobic Sewer Biofilms by Ferric Iron Dosing. *Water Res.* **2009**, *43*, 4123–4132.
- (4) Zhang, C.; Huang, J.; Zhang, J.; Liu, S.; Cui, M.; An, B.; Wang, X.; Pu, J.; Zhao, T.; Fan, C.; Lu, T. K.; Zhong, C. Engineered *Bacillus Subtilis* Biofilms as Living Glues. *Mater. Today* **2019**, *28*, 40–48.
- (5) Duraj-Thatte, A. M.; Manjula-Basavanna, A.; Courchesne, N. M. D.; Cannici, G. I.; Sánchez-Ferrer, A.; Frank, B. P.; van't Hag, L.; Cotts, S. K.; Fairbrother, D. H.; Mezzenga, R.; Joshi, N. S. Water-Processable, Biodegradable and Coatable Aquaplastic from Engineered Biofilms. *Nat. Chem. Biol.* **2021**, *17*, 732–738.
- (6) Balasubramanian, S.; Aubin-Tam, M.-E.; Meyer, A. S. 3D Printing for the Fabrication of Biofilm-Based Functional Living Materials. *ACS Synth. Biol.* **2019**, *8*, 1564–1567.
- (7) Schaffner, M.; Rühs, P. A.; Coulter, F.; Kilcher, S.; Studart, A. R. 3D Printing of Bacteria into Functional Complex Materials. *Sci. Adv.* **2017**, *3* (12), No. eaao6804.
- (8) Limoli, D. H.; Jones, C. J.; Wozniak, D. J. Bacterial Extracellular Polysaccharides in Biofilm Formation and Function. *Microbiol. Spectr.* **2015**, *3*, 1–30.

- (9) Fong, J. N. C.; Yildiz, F. H. Bio Fi Lm Matrix Proteins. *Microbiol. Spectr.* **2015**, *3*, 201–222.
- (10) Flemming, H.-C.; Wingender, J.; Szewzyk, U.; Steinberg, P.; Rice, S. A.; Kjelleberg, S. Biofilms: An Emergent Form of Bacterial Life. *Nat. Rev. Microbiol.* **2016**, *14*, 563–575.
- (11) Mann, E. E.; Wozniak, D. J. Pseudomonas Biofilm Matrix Composition and Niche Biology. *FEMS Microbiol. Rev.* **2012**, *36*, 893–916.
- (12) Erskine, E.; MacPhee, C. E.; Stanley-Wall, N. R. Functional Amyloid and Other Protein Fibers in the Biofilm Matrix. *J. Mol. Biol.* **2018**, *430*, 3642–3656.
- (13) Barnhart, M. M.; Chapman, M. R. Curli Biogenesis and Function. *Annu. Rev. Microbiol.* **2006**, *60*, 131–147.
- (14) Thongsomboon, W.; Serra, D. O.; Possling, A.; Hadjineophytou, C.; Hengge, R.; Cegelski, L. Phosphoethanolamine Cellulose: A Naturally Produced Chemically Modified Cellulose. *Science* **2018**, *359*, 334–338.
- (15) Jeffries, J.; Thongsomboon, W.; Visser, J. A.; Enriquez, K.; Yager, D.; Cegelski, L. Variation in the Ratio of Curli and Phosphoethanolamine Cellulose Associated with Biofilm Architecture and Properties. *Biopolymers* **2021**, *112*, 1–11.
- (16) Ziege, R.; Tsirigoni, A.-M.; Large, B.; Serra, D. O.; Blank, K. G.; Hengge, R.; Fratzl, P.; Bidan, C. M. Adaptation of Escherichia Coli Biofilm Growth, Morphology, and Mechanical Properties to Substrate Water Content. *ACS Biomater. Sci. Eng.* **2021**, *7*, 5315–5325.
- (17) Rühls, P. A.; Böni, L.; Fuller, G. G.; Inglis, R. F.; Fischer, P. In-Situ Quantification of the Interfacial Rheological Response of Bacterial Biofilms to Environmental Stimuli. *PLoS One* **2013**, *8*, No. e78524.
- (18) Degtyar, E.; Harrington, M. J.; Politi, Y.; Fratzl, P. The Mechanical Role of Metal Ions in Biogenic Protein-Based Materials. *Angew. Chem., Int. Ed.* **2014**, *53*, 12026–12044.
- (19) Ukmar-Godec, T. Mineralization of Goethite in Limpet Radular Teeth. In *Iron Oxides*; Faivre, D., Ed.; Wiley, 2016; pp 207–224.
- (20) Chan, C. S.; Fakra, S. C.; Edwards, D. C.; Emerson, D.; Banfield, J. F. Iron Oxhydroxide Mineralization on Microbial Extracellular Polysaccharides. *Geochim. Cosmochim. Acta* **2009**, *73*, 3807–3818.
- (21) Fratzl, P.; Gupta, H. S.; Paschalis, E. P.; Roschger, P. Structure and Mechanical Quality of the Collagen–Mineral Nano-Composite in Bone. *J. Mater. Chem.* **2004**, *14*, 2115–2123.
- (22) Baumgartner, J.; Faivre, D. Magnetite Biomineralization in Bacteria. *Prog. Mol. Subcell. Biol.* **2011**, *52*, 3–27.
- (23) Jehle, F.; Fratzl, P.; Harrington, M. J. Metal-Tunable Self-Assembly of Hierarchical Structure in Mussel-Inspired Peptide Films. *ACS Nano* **2018**, *12*, 2160–2168.
- (24) Khare, E.; Holten-Andersen, N.; Buehler, M. J. Transition-Metal Coordinate Bonds for Bioinspired Macromolecules with Tunable Mechanical Properties. *Nat. Rev. Mater.* **2021**, *6*, 421–436.
- (25) Mosharaf, M. K.; Tanvir, M. Z. H.; Haque, M. M.; Haque, M. A.; Khan, M. A. A.; Molla, A. H.; Alam, M. Z.; Islam, M. S.; Talukder, M. R. Metal-Adapted Bacteria Isolated from Wastewaters Produce Biofilms by Expressing Proteinaceous Curli Fimbriae and Cellulose Nanofibers. *Front. Microbiol.* **2018**, *9*, 1–17.
- (26) Tallawi, M.; Opitz, M.; Lieleg, O. Modulation of the Mechanical Properties of Bacterial Biofilms in Response to Environmental Challenges. *Biomater. Sci.* **2017**, *5*, 887–900.
- (27) Klotz, M.; Kretschmer, M.; Goetz, A.; Ezendam, S.; Lieleg, O.; Opitz, M. Importance of the Biofilm Matrix for the Erosion Stability of Bacillus Subtilis NCIB 3610 Biofilms. *RSC Adv.* **2019**, *9*, 11521–11529.
- (28) Serra, D. O.; Richter, A. M.; Hengge, R. Cellulose as an Architectural Element in Spatially Structured Escherichia Coli Biofilms. *J. Bacteriol.* **2013**, *195*, 5540–5554.
- (29) Hayashi, K.; Morooka, N.; Yamamoto, Y.; Fujita, K.; Isono, K.; Choi, S.; Ohtsubo, E.; Baba, T.; Wanner, B. L.; Mori, H.; Horiuchi, T. Highly Accurate Genome Sequences of Escherichia Coli K-12 Strains MG1655 and W3110. *Mol. Syst. Biol.* **2006**, *2*, 2006.
- (30) Jubelin, G.; Vianney, A.; Beloin, C.; Ghigo, J.-M.; Lazzaroni, J.-C.; Lejeune, P.; Dorel, C. CpxR/OmpR Interplay Regulates Curli Gene Expression in Response to Osmolarity in Escherichia Coli. *J. Bacteriol.* **2005**, *187*, 2038–2049.
- (31) Lieleg, O.; Caldara, M.; Baumgärtel, R.; Ribbeck, K. Mechanical Robustness of Pseudomonasaeruginosa Biofilms. *Soft Matter* **2011**, *7*, 3307.
- (32) Stanley-Gray, J.; Zhang, Z.; Venkataraman, D. Updated Coordination Geometry Table of the D-Block Elements and Their Ions. *J. Chem. Educ.* **2021**, *98*, 2476–2481.
- (33) Bhardwaj, N. C.; Jadon, S. C. S.; Singh, R. V. Aluminium(III) Complexes with Usual and Unusual Coordination Numbers. *Synth. React. Inorg. Met. Chem.* **1994**, *24*, 1267–1279.
- (34) Katz, A. K.; Glusker, J. P.; Beebe, S. A.; Bock, C. W. Calcium Ion Coordination: A Comparison with That of Beryllium, Magnesium, and Zinc. *J. Am. Chem. Soc.* **1996**, *118*, 5752–5763.
- (35) Horvat, M.; Pannuri, A.; Romeo, T.; Dogsa, I.; Stopar, D. Viscoelastic Response of Escherichia Coli Biofilms to Genetically Altered Expression of Extracellular Matrix Components. *Soft Matter* **2019**, *15*, 5042–5051.
- (36) Kretschmer, M.; Lieleg, O. Chelate Chemistry Governs Ion-Specific Stiffening of: Bacillus Subtilis B-1 and Azotobacter Vinelandii Biofilms. *Biomater. Sci.* **2020**, *8*, 1923–1933.
- (37) Periasamy, S.; Nair, H. A. S.; Lee, K. W. K.; Ong, J.; Goh, J. Q. J.; Kjelleberg, S.; Rice, S. A. Pseudomonas Aeruginosa PAO1 Exopolysaccharides Are Important for Mixed Species Biofilm Community Development and Stress Tolerance. *Front. Microbiol.* **2015**, *6*, 1–10.
- (38) Li, W.-W.; Yu, H.-Q. Insight into the Roles of Microbial Extracellular Polymer Substances in Metal Biosorption. *Bioresour. Technol.* **2014**, *160*, 15–23.
- (39) Quintelas, C.; Rocha, Z.; Silva, B.; Fonseca, B.; Figueiredo, H.; Tavares, T. Removal of Cd(II), Cr(VI), Fe(III) and Ni(II) from Aqueous Solutions by an E. Coli Biofilm Supported on Kaolin. *Chem. Eng. J.* **2009**, *149*, 319–324.
- (40) Božič, M.; Liu, P.; Mathew, A. P.; Kokol, V. Enzymatic Phosphorylation of Cellulose Nanofibers to New Highly-Ions Adsorbing, Flame-Retardant and Hydroxyapatite-Growth Induced Natural Nanoparticles. *Cellulose* **2014**, *21*, 2713–2726.
- (41) Oshima, T.; Kondo, K.; Ohto, K.; Inoue, K.; Baba, Y. Preparation of Phosphorylated Bacterial Cellulose as an Adsorbent for Metal Ions. *React. Funct. Polym.* **2008**, *68*, 376–383.
- (42) Hosny, W. M.; Basta, A. H.; El-Saied, H. Metal Chelates with Some Cellulose Derivatives: Synthesis and V. Characterization of Some Iron(III) Complexes with Cellulose Ethers. *Polym. Int.* **1997**, *42*, 157.
- (43) Hidalgo, G.; Chen, X.; Hay, A. G.; Lion, L. W. Curli Produced by Escherichia Coli Phl628 Provide Protection from Hg(II). *Appl. Environ. Microbiol.* **2010**, *76*, 6939–6941.
- (44) House, E.; Collingwood, J.; Khan, A.; Korchazkina, O.; Berthon, G.; Exley, C. Aluminium, Iron, Zinc and Copper Influence the in Vitro Formation of Amyloid Fibrils of A β 42 in a Manner Which May Have Consequences for Metal Chelation Therapy in Alzheimer's Disease. *J. Alzheimer's Dis.* **2004**, *6*, 291–301.
- (45) Mujika, J. I.; Rodríguez-Guerra Pedregal, J.; Lopez, X.; Ugalde, J. M.; Rodríguez-Santiago, L.; Sodupe, M.; Maréchal, J.-D. Elucidating the 3D Structures of Al(III)–A β Complexes: A Template Free Strategy Based on the Pre-Organization Hypothesis. *Chem. Sci.* **2017**, *8*, 5041–5049.
- (46) Faller, P.; Hureau, C. Bioinorganic Chemistry of Copper and Zinc Ions Coordinated to Amyloid- β Peptide. *Dalt. Trans.* **2009**, *7*, 1080–1094.
- (47) Hureau, C. Coordination of Redox Active Metal Ions to the Amyloid Precursor Protein and to Amyloid- β Peptides Involved in Alzheimer Disease. Part 1: An Overview. *Coord. Chem. Rev.* **2012**, *256*, 2164–2174.
- (48) Nair, N. G.; Perry, G.; Smith, M. A.; Reddy, V. P. NMR Studies of Zinc, Copper, and Iron Binding to Histidine, the Principal Metal

Ion Complexing Site of Amyloid- β Peptide. *J. Alzheimer's Dis.* **2010**, *20*, 57–66.

(49) Jumper, J.; Evans, R.; Pritzel, A.; Green, T.; Figurnov, M.; Ronneberger, O.; Tunyasuvunakool, K.; Bates, R.; Žídek, A.; Potapenko, A.; Bridgland, A.; Meyer, C.; Kohl, S. A. A.; Ballard, A. J.; Cowie, A.; Romera-Paredes, B.; Nikolov, S.; Jain, R.; Adler, J.; Back, T.; Petersen, S.; Reiman, D.; Clancy, E.; Zielinski, M.; Steinegger, M.; Pacholska, M.; Berghammer, T.; Bodenstein, S.; Silver, D.; Vinyals, O.; Senior, A. W.; Kavukcuoglu, K.; Kohli, P.; Hassabis, D. Highly Accurate Protein Structure Prediction with AlphaFold. *Nature* **2021**, *596*, 583–589.

(50) Varadi, M.; Anyango, S.; Deshpande, M.; Nair, S.; Natassia, C.; Yordanova, G.; Yuan, D.; Stroe, O.; Wood, G.; Laydon, A.; Žídek, A.; Green, T.; Tunyasuvunakool, K.; Petersen, S.; Jumper, J.; Clancy, E.; Green, R.; Vora, A.; Lutfi, M.; Figurnov, M.; Cowie, A.; Hobbs, N.; Kohli, P.; Kleywegt, G.; Birney, E.; Hassabis, D.; Velankar, S. AlphaFold Protein Structure Database: Massively Expanding the Structural Coverage of Protein-Sequence Space with High-Accuracy Models. *Nucleic Acids Res.* **2022**, *50*, D439–D444.

(51) Manning, G. S. Limiting Laws and Counterion Condensation in Polyelectrolyte Solutions I. Colligative Properties. *J. Chem. Phys.* **1969**, *51*, 924–933.

(52) Manning, G. S. Counterion Condensation on Charged Spheres, Cylinders, and Planes. *J. Phys. Chem. B* **2007**, *111*, 8554–8559.

(53) van Gestel, J.; Weissing, F. J.; Kuipers, O. P.; Kovács, Á. T. Density of Founder Cells Affects Spatial Pattern Formation and Cooperation in *Bacillus Subtilis* Biofilms. *ISME J.* **2014**, *8*, 2069–2079.

(54) Lambert, G.; Bergman, A.; Zhang, Q.; Bortz, D.; Austin, R. Physics of Biofilms: The Initial Stages of Biofilm Formation and Dynamics. *New J. Phys.* **2014**, *16*, 045005.

(55) Deng, C.; Li, X.; Xue, X.; Pashley, R. M. The Effects of Low Levels of Trivalent Ions on a Standard Strain of *Escherichia Coli* (ATCC 11775) in Aqueous Solutions. *Microbiologyopen* **2018**, *7*, No. e00574.

(56) Teitzel, G. M.; Parsek, M. R. Heavy Metal Resistance of Biofilm and Planktonic *Pseudomonas Aeruginosa*. *Appl. Environ. Microbiol.* **2003**, *69*, 2313–2320.

(57) Epstein, W.; Schultz, S. G. Cation Transport in *Escherichia Coli*. *J. Gen. Physiol.* **1965**, *49*, 221–234.

(58) Flory, P. J.; Rehner, J. Statistical Mechanics of Cross-Linked Polymer Networks II. Swelling. *J. Chem. Phys.* **1943**, *11*, 521–526.

Recommended by ACS

Failure Analysis of Cement Sheath Mechanical Integrity Based on the Statistical Damage Variable

Xuning Wu, Rui Chen, *et al.*

JANUARY 06, 2023
ACS OMEGA

READ 

Highly Dispersed Cu Produced by Mechanical Stress-Activated Redox Reaction to Establish Galvanic Corrosion in Fe Implant

Chongxian He, Cijun Shuai, *et al.*

DECEMBER 26, 2022
ACS BIOMATERIALS SCIENCE & ENGINEERING

READ 

Degradable Biocompatible Porous Microtube Scaffold for Extended Donor Cell Survival and Activity

Helen Nguyen, David J. Lundy, *et al.*

JANUARY 03, 2023
ACS BIOMATERIALS SCIENCE & ENGINEERING

READ 

Poly β -Cyclodextrin/Quaternary Ammoniated Chitosan Cryogel with a Porous Structure for Effective Hemostasis

Min Tan, Sheng Zhang, *et al.*

JANUARY 09, 2023
ACS BIOMATERIALS SCIENCE & ENGINEERING

READ 

Get More Suggestions >